



Research papers

Soil erosion and transport simulation and critical erosion area identification in a headwater catchment contaminated by the Fukushima nuclear accident



Lezhang Wei^{a,b,*}, Tsuyoshi Kinouchi^a, Mark L. Velleux^c, Teppei Omata^a, Keiichi Takahashi^a, Megumi Araya^a

^a Department of Environmental Science and Technology, Tokyo Institute of Technology, Japan

^b Linköping University – Guangzhou University Research Center on Urban Sustainable Development, Guangzhou University, China

^c HDR, United States

ARTICLE INFO

Keywords:

Soil erosion
Multiple solid particle size classes
Critical erosion areas
TRES model
Kuchibuto River catchment

ABSTRACT

Radiocesium released by the accident at the Fukushima Dai-ichi Nuclear Power Plant in 2011 contaminated a large land surface area. Due to the strong and size-dependent adsorption capability of soil particles to radionuclides, a better understanding of erosion and transport of soil particles and identification of erosion prone areas within watersheds are significant for contaminant management. For this purpose, we simulated soil erosion and transport in a partially forested catchment for multiple particle size classes. Critical erosion areas were identified by the spatial distribution of net soil erosion. Comparisons between simulated and measured suspended solids concentration at multiple locations throughout the catchment demonstrated successful model performance. For the period Mar. 12, 2011 through Dec. 31, 2014, model results indicated that 5500 tonnes of clay, 52000 tonnes of silt, and 22000 tonnes of sand are transported from the catchment. The results showed that soil erosion in the middle part of the catchment is greater mainly because of steep slopes and large fraction of agricultural lands. These simulations suggest that soil decontamination of erosion-prone agricultural lands in the mid-catchment areas would be effective in reducing radiocesium migration with soil particles.

1. Introduction

The Tohoku earthquake in Japan occurred on March 11, 2011. Subsequent explosions at the Fukushima Dai-ichi Nuclear Power Plant (FDNPP) released an estimated 153 PBq ¹³¹I and 13 PBq ¹³⁷Cs to the atmosphere between March 21 and April 5, 2011 (Chino et al., 2011). Radionuclides were deposited onto the land surface and incorporated into surface soils. Among all kinds of radionuclides emitted during the accident, ¹³⁷Cs will persist for the longest time because of its long half-life. Airborne monitoring surveys show radiocesium was widely distributed across forested, agricultural, and residential areas of a large portion of the Abukuma watershed near the FDNPP (MEXT, 2013). Soil erosion generated by localized rainfall events and frequent typhoons is a driving force for radiocesium transport across the landscape. Soil particles to which radionuclides have sorbed are the transmission media of primary concern (Yamashiki et al., 2014). Thus, soil erosion and transport must be quantified to better understand the behavior and fate of radiocesium at the watershed scale.

Process-based watershed soil erosion models can represent fluvial transport associated with the detachment, transport, and deposition of

soil particles caused by rainfall and surface flow throughout a catchment (Lee et al., 2013). In recent decades, a number of soil erosion modeling tools have been developed, including models such as EUROSEM (Morgan et al., 1998), WEPP (Flanagan and Nearing 1995), KINEROS (Woolhiser et al., 1990), SWAT (Srinivasan and Arnold, 1994), and DYRIM (Wang et al., 2007, 2015). Such models can be used to identify critical erosion areas that deliver disproportionately high amounts of sediments and associated contaminants relative to other locations. Identification of those areas most susceptible to erosion can aid development of mitigation strategies and evaluate the effectiveness of best management practices to control nonpoint source pollution, thereby providing a means to prioritize decontamination efforts and evaluate future radiocesium transport (Kumar and Mishra, 2015; Sardar et al., 2014; Tripathi et al. 2003; White et al. 2009; Wu and Chen, 2012, 2013).

Although modeling studies of soil erosion and radiocesium transport for the Fukushima area were conducted after the nuclear accident, earlier studies were limited because they either did not consider the size distribution and differential transport of soil particles associated with radiocesium transport (Tanaka et al. 2013; Kinouchi et al. 2015) or

* Corresponding author at: Guangzhou University, China.
E-mail address: bjyq_2006@126.com (L. Wei).

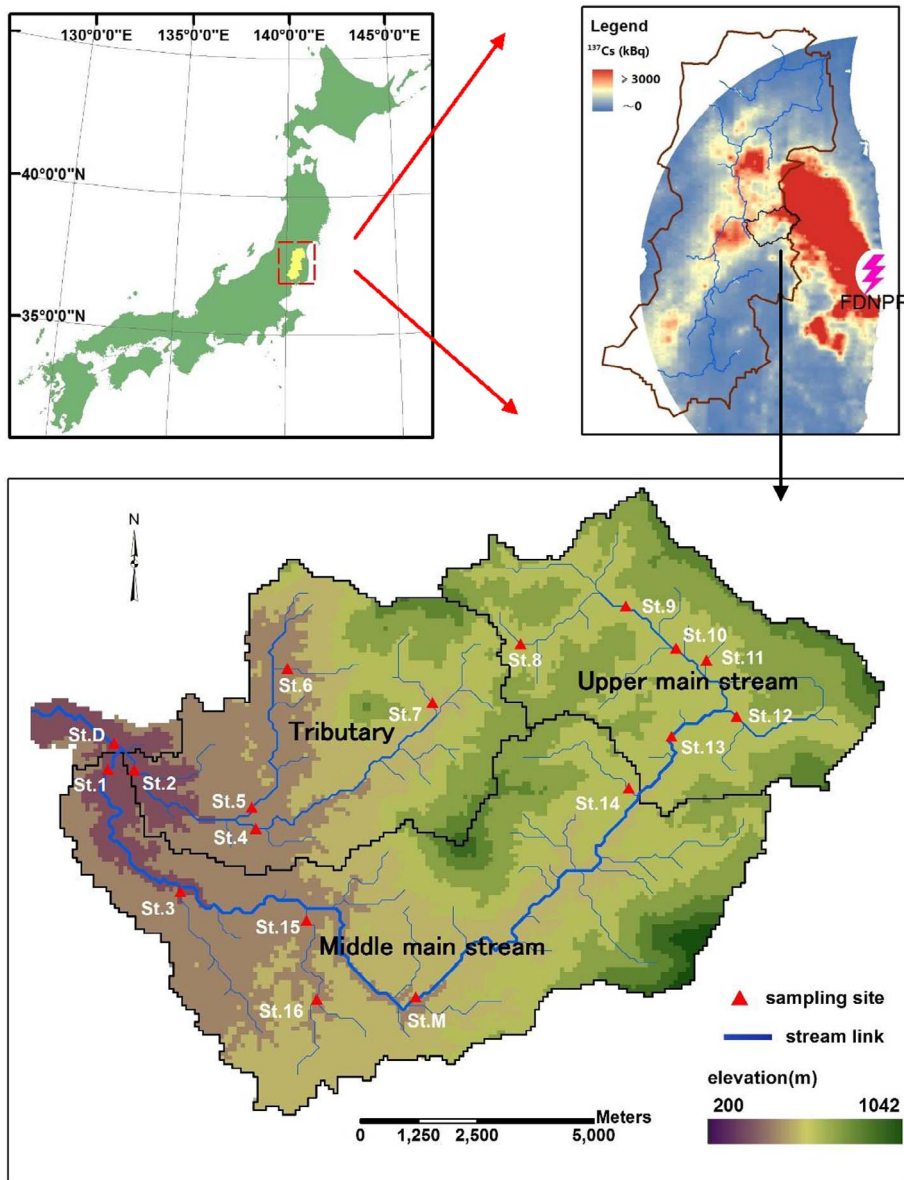


Fig. 1. Outline of the Kuchibuto River catchment (The inventory of ^{137}Cs was obtained from the 3rd airborne monitoring survey by MEXT (2013)).

simulated sediment-radiocesium transport at annual time-scales (Yamaguchi et al. 2013, 2014). Transport by different particle sizes is important because radionuclides sorption to soils is size-dependent, with preferential sorption to finer particles that have higher specific surface areas (He and Walling, 1996; Tanaka et al., 2014). Moreover, soil erosion and transport through fluvial systems is episodic and varies widely over time such that analyses on fine temporal scales are needed to trace water-sediment-radiocesium dynamics for each event. In contrast, sediment measurements in prior studies were limited to a few events or other relatively short timeframes.

Given limitations of prior studies, the objectives of this study were to: (1) simulate soil erosion and transport processes for multiple particle size classes; (2) calibrate and validate the model using nearly 4-year measurements in the study catchment; and (3) identify critical erosion areas within the catchment based on simulated spatial distributions of soil erosion.

2. Study area

The study area is the Kuchibuto River catchment, which is a head-water catchment in the Abukuma River watershed (Fig. 1). High ^{137}Cs

activities have been monitored in this catchment. A consequence of soil erosion and fluvial transport, radioactive substances have been delivered to the more populated downstream regions that lead to the Pacific Ocean. The catchment area is 137 km² with elevations that range from 200 m above sea level at the catchment outlet to 1000 m in the parts of the catchment and an average slope of approximately 9°. The predominant land use is forest, followed by agriculture (i.e. paddy fields and farm land), and a very small portion of urban area (Fig. 2). Four soil types, evolved mainly from granitic parent materials, cover the catchment: kuroboku soil, granitic forest soil, lowland soil, and gley soil.

3. Data collection

Spatial data includes topographic, land use, and soil properties data. A Shuttle Radar Topography Mission (SRTM) based 90-meter Digital Elevation Model (DEM) data was downloaded (<http://glcf.umd.edu/data/srtm/>) and used to generate slope, flow direction, flow accumulation, river links and sub catchment boundaries (Fig. 1). Stream channel geometry (width, bank height, etc.) was defined as measured by a field survey in 2013. A sandy bed was assumed for the initial condition of stream bed materials since steep bed slopes are dominant

Fig. 2. Land use in the Kuchibuto River catchment.

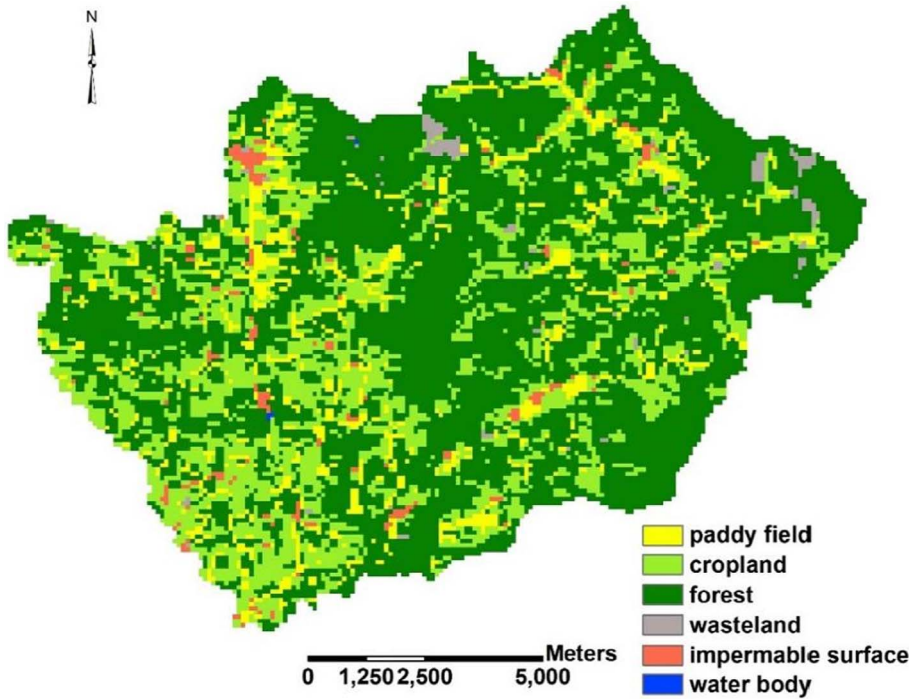


Table 1
Parameters for sand, silt and clay.

Solid types	d_p (μm)	G (-)	V_s (cm/s)	C_f (-)	β (-)	C_h (m^{-1})	α (-)	Ω_0 (m/s)
Sand (> 63 μm)	100	2.65	0.8	850	0.001	150	0.335	0.004
Silt (3–63 μm)	20	2.65	0.0385	1500	0.0035	150	0.335	0.004
Clay (< 3 μm)	2	2.65	0.0004	70	0.000003	150	0.335	0.004

* C_h , α and Ω_0 were determined by referring to Kinouchi et al. (2015), Morgan et al.(1998) and Woolhiser et al. (1990), respectively

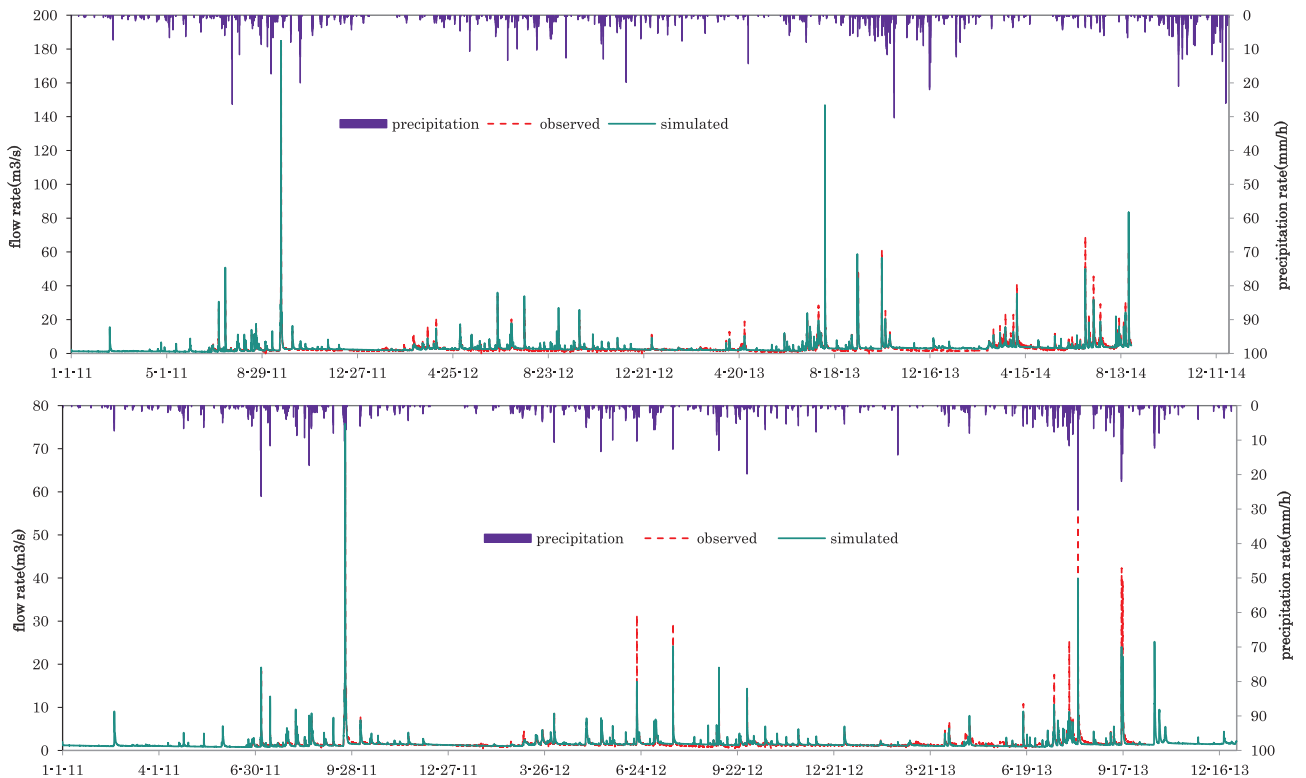


Fig. 3. Simulated and observed flow rates at the downstream site (top) and middle stream site (bottom).

Table 2
Evaluation criteria of simulated flow rate.

Location	Coefficient	2011	2012	2013	2014
Downstream (St. D)	NSE	0.93	0.69	0.91	0.80
	RSR	0.26	0.56	0.30	0.45
	PBIAS	-9%	-18%	-17%	11%
Middle stream (St. M)	NSE	0.96	0.62	0.80	-
	RSR	0.20	0.62	0.45	-
	PBIAS	5%	-10%	14%	-

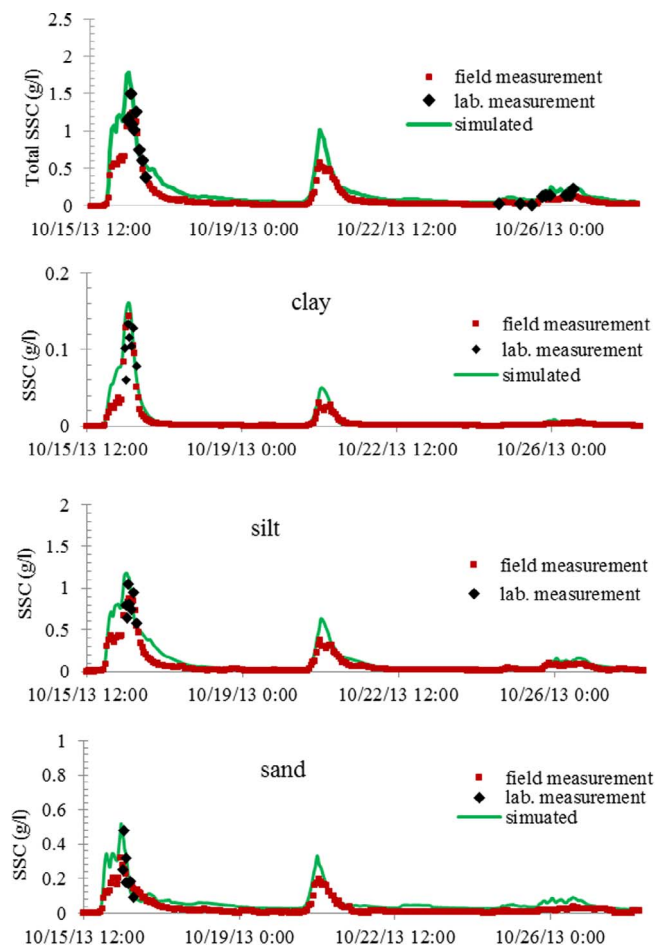


Fig. 4a. SSC at the downstream site (St. D) for the event during Oct. 15–26, 2013. (SSC of field measurement is the conversion from measured turbidity, and SSC of lab. measurement is the concentration of grab water samples analyzed in the laboratory).

in this headwater catchment. Land use and soil data were obtained from the Japan Ministry of Land, Infrastructure, Transport, and Tourism (MLIT) (<http://nlftp.mlit.go.jp/ksj/>). Radar precipitation data from the Japan Meteorological Agency (JMA) were used to specify rainfall inputs in the model. Rainfall intensity was assumed to be uniform within a grid cell which has 1 km spatial resolution. The native resolution of land use and soil type data are approximately 100 m and 1000 m, respectively. Those data were resampled into 90-m spatial resolution using the majority resampling function included in ArcGIS (fractions of each soil type remained almost the same after resampling).

Site measurements include stream discharge, suspended sediment concentration (SSC) and solid particle size distribution (PSD). In total, there were 18 monitoring sites in the river channel within the catchment. Station D (St. D) and Station M (St. M), at the down main stream site and middle main stream site respectively for long term water levels and turbidity observation (Fig. 1). Water levels and turbidity have been monitored at 10-minute intervals at these two stations since June 2011.

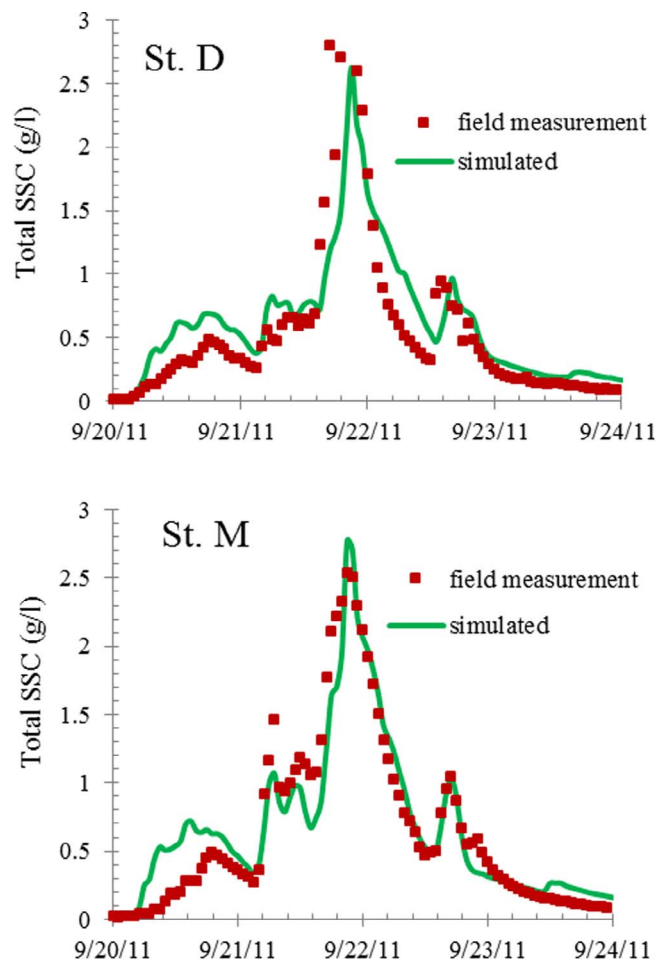


Fig. 4a. (continued)

These measurements are surrogates for flow rate and SSC. Water levels were monitored using a pressure-transducer and were converted to flow rates using a rating curve. Turbidity was monitored by an optical sensor (MacVan Analite turbidity meter, 3000-NTU). Turbidity meter output (in mV) was converted to SSC (in g/l) based on a relationship between turbidity and laboratory analyses of SSC in stream water samples collected by Kinouchi et al. (2015), Yoshimura et al. (2015) and other data collected by researchers at the University of Tsukuba. Additional data to define the relationship between turbidity and SSC were obtained from SSC and turbidity measurements performed as part of this study (JFE-Advantec Infinity turbidity meter). During March and October 2013, suspended solid particle-size distributions were monitored at the downstream site using a Sequoia Scientific LISST-Streamside meter to measure the volume of 24 particle size classes ranging in diameter from 1.89 to 386.38 μm . The mass fraction of each size class was estimated from the measured volume fraction assuming a particle density of 2.65 kg/l. Thus, the SSC of each solid type can be determined from total SSC by multiplying it by mass fraction of each size class. Furthermore, SSC and flow rate were used to estimate the flux of each particle size class.

4. Methods

The Two-Dimensional Runoff Erosion and Export (TRES) watershed model (Velleux et al., 2008), which was derived from the earlier C-ASC2D framework (Julien et al., 1995; Johnson et al., 2000), is an event-based, distributed model that can simulate hydrological processes, soil erosion, and chemical transport at the watershed scale. Wei and Kinouchi (2014) improved the TRES framework to simulate

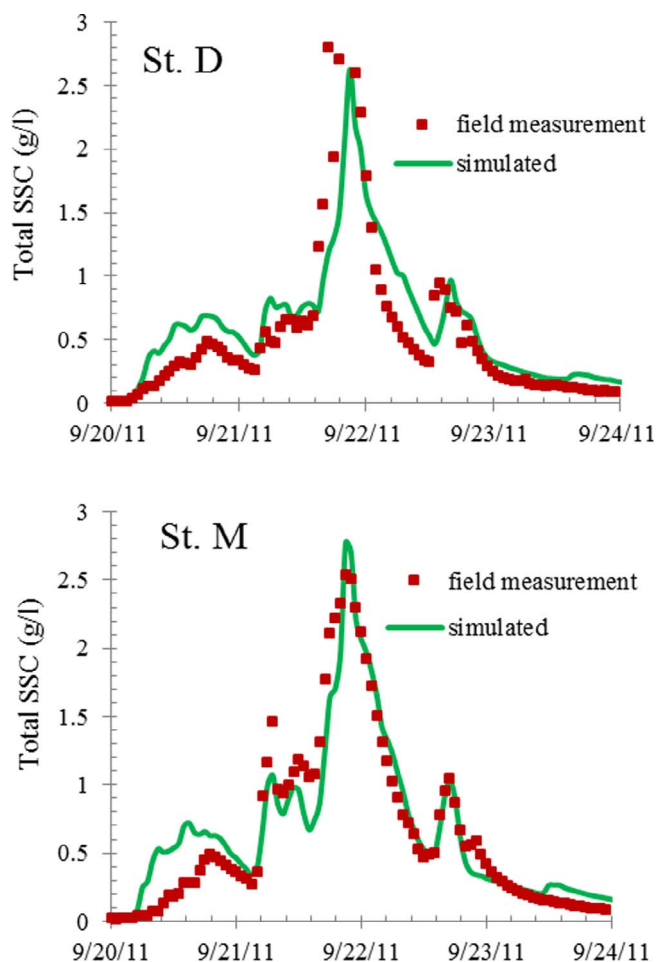


Fig. 4b. Total SSC at the downstream site (St. D) and the middle stream site (St. M) for the event during Sep. 20–24, 2011.

continuous hydrologic processes. The major components of the hydrological model include: rainfall, interception and evapotranspiration, surface storage, infiltration, subsurface and groundwater flow, and overland and channel runoff routing (Velleux et al., 2008; Wei and Kinouchi, 2014). Overland flow is simulated in two dimensions using the diffusive wave approximation. In floodplain areas, water and transported constituents (e.g. sediment) are transferred between the overland plane and channel network based on the difference in water surface elevations. Channel flow is simulated in one dimension using the diffusive wave approximation. Methods to simulate soil erosion and transport in the model are described as follows.

4.1. Soil erosion and transport for the overland plane

The governing equation for upland soil erosion and transport is expressed as

$$\frac{\partial AC_s}{\partial t} + \frac{\partial C_s q_x}{\partial x} + \frac{\partial C_s q_y}{\partial y} = e_s + e_h \quad (1)$$

where, A is the cross-sectional area of the overland flow (m^2), C_s is suspended sediment concentration in overland flow (kg/m^3), q_x , q_y are the unit discharge in x - or y -directions (m^2/s), respectively, e_s is splash erosion by rainfall ($kg/s/m$); e_h is net erosion by water flow ($kg/s/m$). Splash erosion of soils can be approximated as a function of the square of the rainfall rate as described by Woolhiser et al. (1990).

$$e_s = (1 - k_v) w \rho_s C_f e^{-C_h h_i^2} \quad (2)$$

where, k_v is the fraction of vegetative cover in each cell (dimensionless);

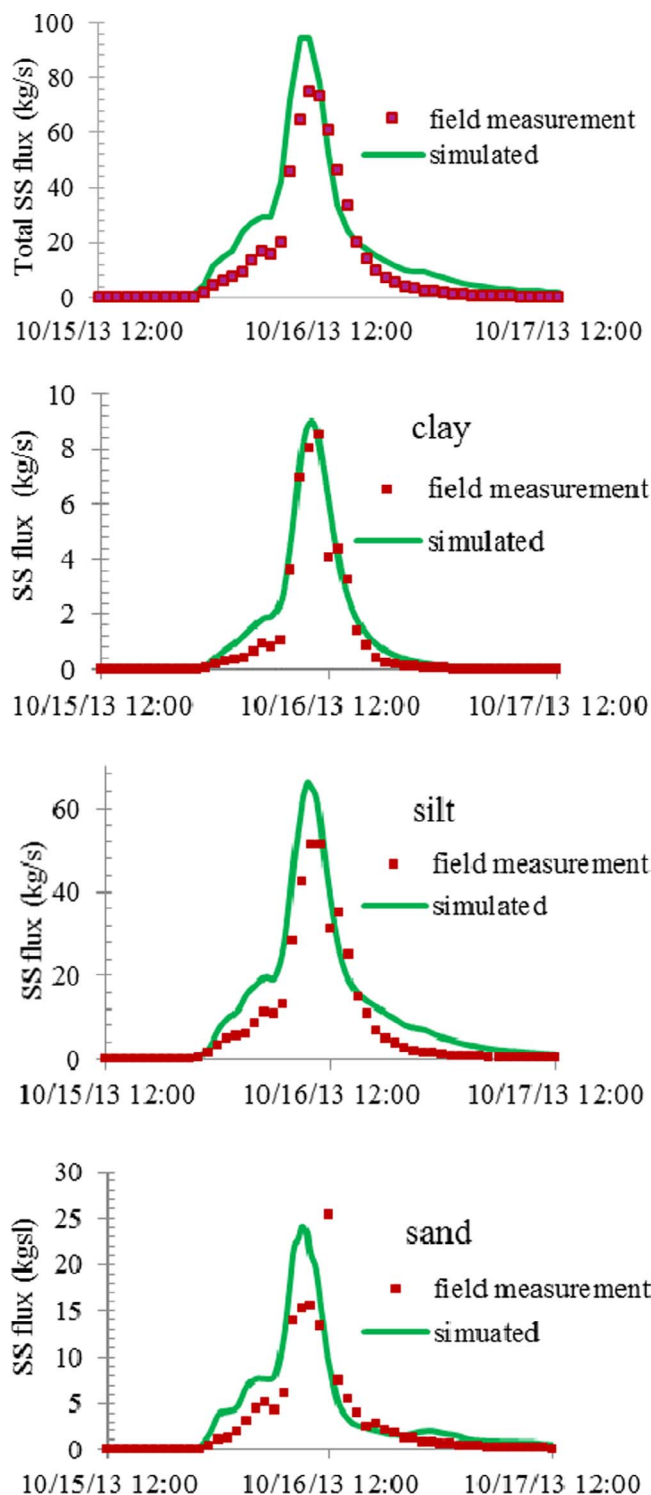


Fig. 5a. Total and fractional SS fluxes at St. D during Oct. 15–17, 2013.

w is cell size (m); ρ_s is solid density (kg/m^3); i_n is net rainfall intensity (m/s); h is surface water depth (m); and C_f , C_h are coefficients (s/m , $1/m$).

Erosion by water flow is the function of transport capacity:

$$e_h = \alpha w v_s (C_m - C_s) \quad (3)$$

where, α is coefficient, when it is net deposition ($C_m < C_s$), α equals to 1, otherwise, it is determined according to soil cohesion (Morgan et al., 1998). v_s is solid settling velocity (m/s), C_m is total sediment transport capacity (kg/m^3). The Engelund and Hansen (1967) equation is used to

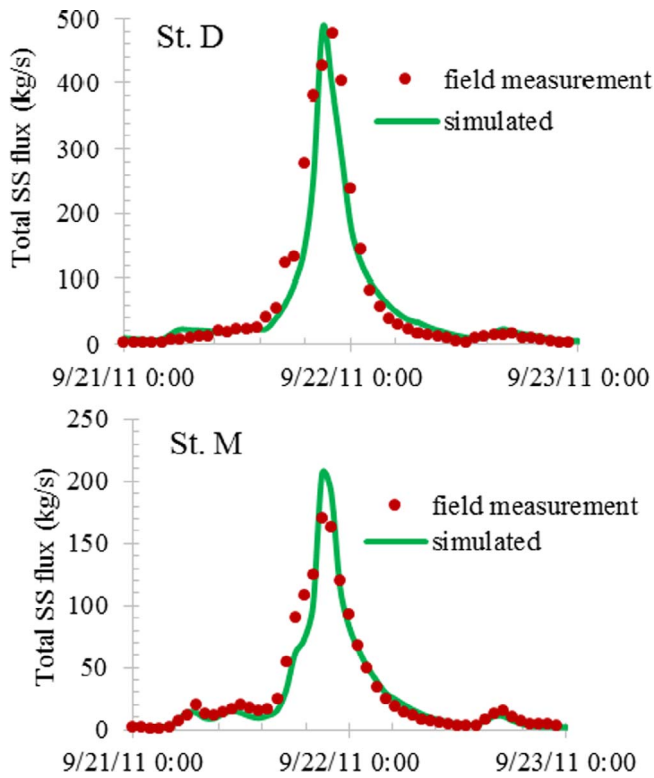


Fig. 5b. Total SS flux at St. D and St. M during Sep. 21–23, 2011.

calculate C_m :

$$C_m = \beta \frac{0.05\rho_s}{d_p(G-1)} \sqrt{\frac{hS_f}{g}} (\mu S_f - \Omega_0) \quad (4)$$

where, S_f is friction slope (dimensionless); μ is flow velocity(m/s); Ω_0 is the threshold unit stream power (m/s); d_p is solid diameter (m); G is particle specific gravity (dimensionless), g is gravitational acceleration (m/s²). Because C_m was developed for experimental flow conditions (e.g. streams, flumes) that differ from the shallow surface runoff, the coefficient β was used as a calibration factor to adjust total sediment transport capacity.

4.2. Sediment erosion and transport in a River channel

The governing equation for sediment erosion and transport in a river channel is expressed as:

$$\frac{\partial AC_s}{\partial t} + \frac{\partial C_s q_x}{\partial x} = J_e - J_d \quad (5)$$

$$J_e = \frac{(J_c - v_a C_s)}{\rho_b} C_{sb} \quad (6)$$

where C_{sb} is concentration of sediment at the bottom boundary (in the bed) [kg/m³], which is updated according to mass balance in each time step, v_a is flow velocity [m/s], ρ_b is bulk density of bed sediments [kg/m³], J_c is sediment transport capacity areal flux [kg/m²/s], which is calculated by:

$$J_c = \frac{v_a C_t}{A} \quad (7)$$

C_t is concentration of entrained sediment particles at the transport capacity (kg/m³), and calculated by:

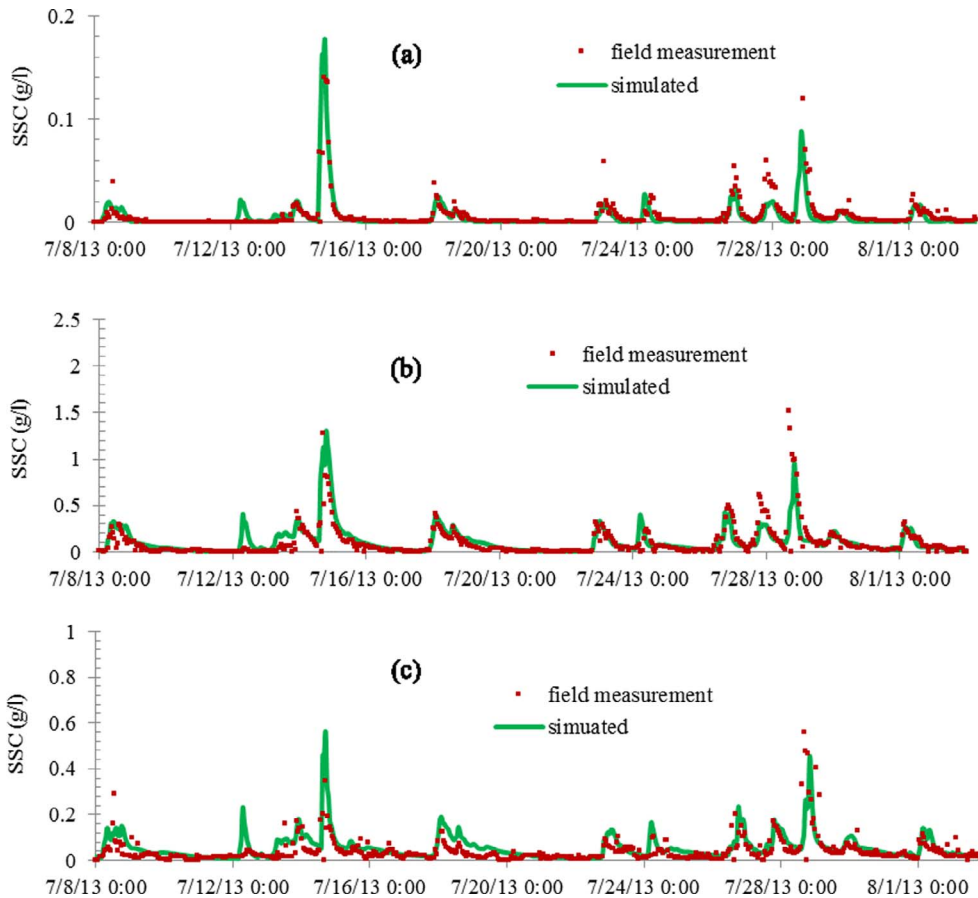


Fig. 6. Comparison of SSSC for (a) clay, (b) silt and (c) sand at the downstream site (St. D) during the period of model validation.

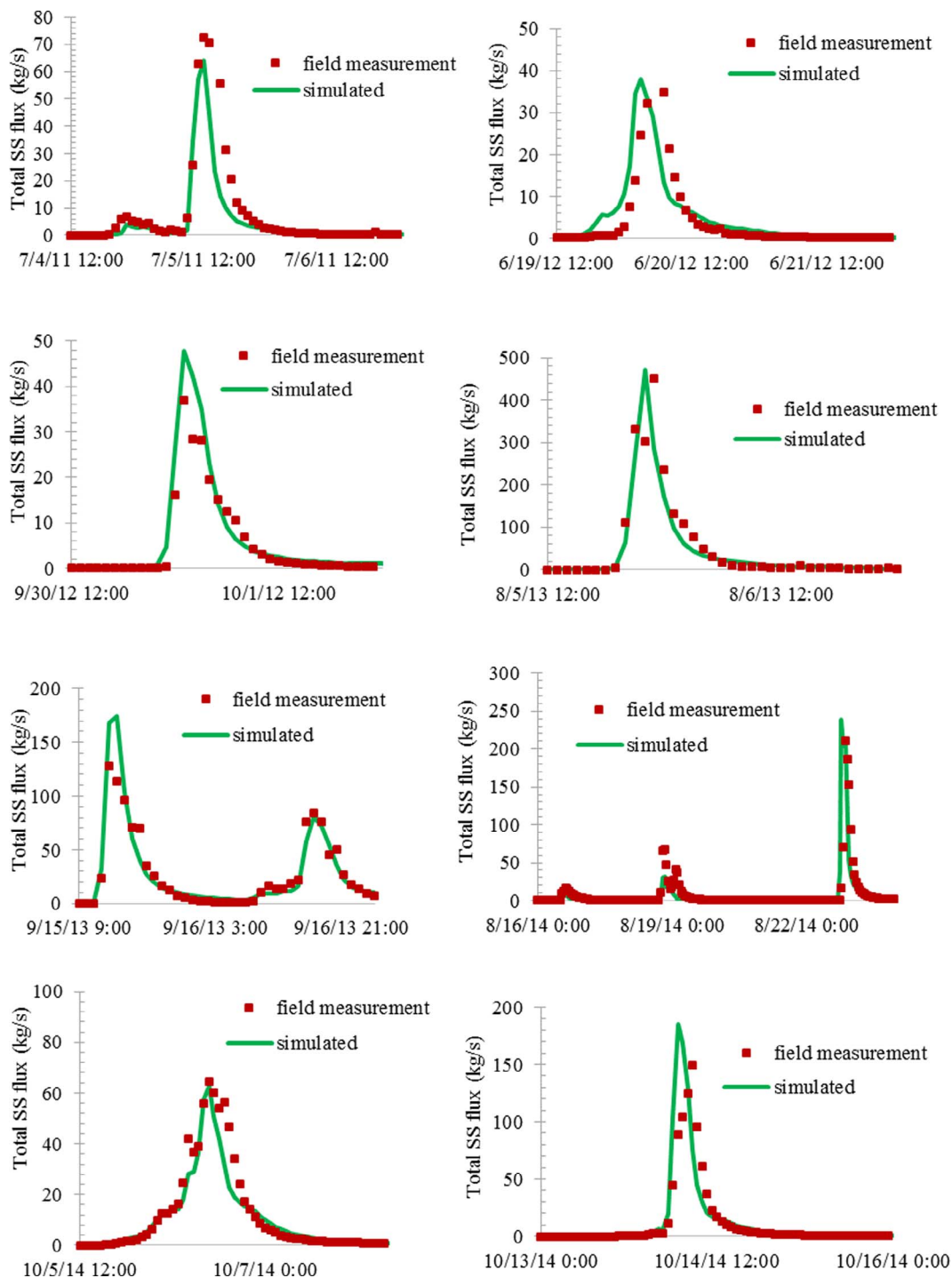


Fig. 7. Comparison of total SS flux at St. D during individual flood events for model validation.

$$C_t = 10^3 \frac{GC_w}{G + (1-G)C_w} \quad (8)$$

$$C_w = 0.05 \left(\frac{G}{G-1} \right) \frac{(v_a - v_c) S_f}{[(G-1)gd_p]^{0.5}} \left[\frac{R_h S_f}{(G-1)gd_p} \right]^{0.5} \quad (9)$$

where, v_c is critical velocity for erosion in the channel (m/s), R_h is hydraulic radius of flow (m).

The deposition flux in the river channel is expressed as a mass rate of particle removal from the water column over time and the concentration of sediment particles:

$$J_d = wv_s P_{dep} C_s \quad (10)$$

where P_{dep} is probability of deposition (dimensionless) (Gessler 1965, 1967, 1971).

For this study, the spectrum of soil particles was simulated as three size classes: sand ($> 63 \mu\text{m}$), silt ($3\text{--}63 \mu\text{m}$) and clay ($< 3 \mu\text{m}$). The model separately calculated the transport of soil particles in each class and did not consider interactions between particles. Representative diameters for particles within each size class are shown in Table 1. Fall velocities calculated according to Stokes' law and which are expected to represent upper bounds for discrete particle settling.

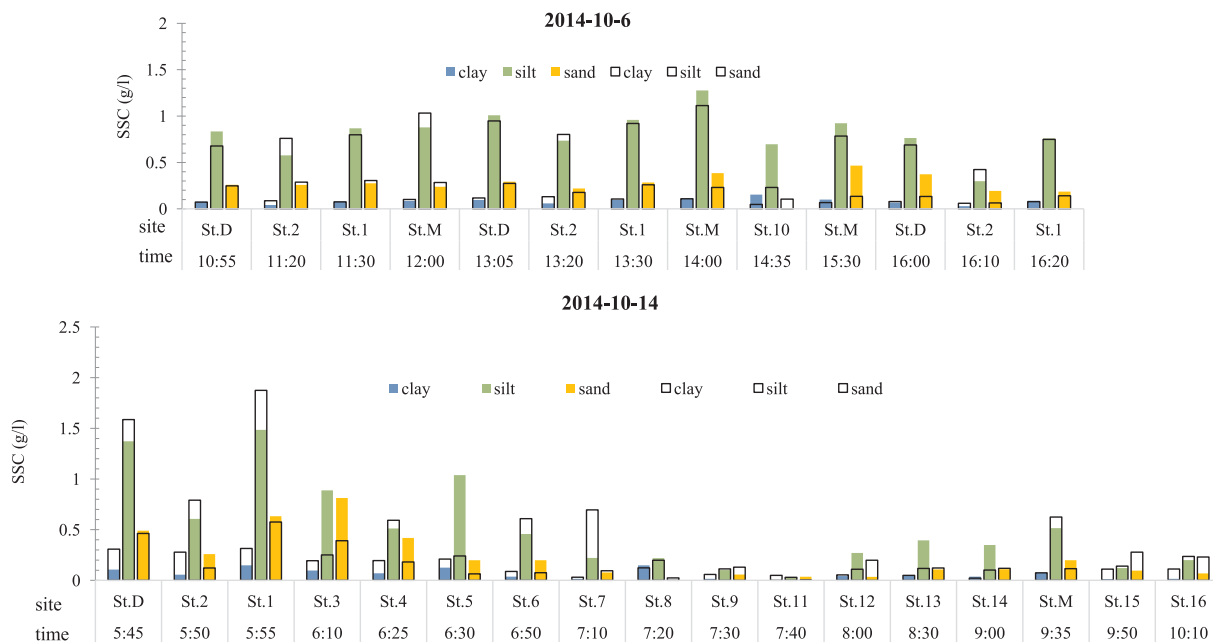


Fig. 8. Comparison of measured and simulated fractional SSCs for multiple sites during two flood events. A color bar and a box represent measured and simulated fractional SSCs, respectively.

4.3. Model evaluation criteria

In this study, three metrics Nash-Sutcliffe Efficiency (*NSE*), RMSE-observation standard deviation ratio (*RSR*), and Percent bias (*PBIAS*) (Moriassi et al. 2007) were used to evaluate simulation results. For a monthly time step, Moriassi et al. (2007) proposed that simulations can be judged as “satisfactory” when $NSE > 0.50$, $RSR < 0.70$, and $|PBIAS| < 25\%$ for streamflow and when $|PBIAS|$ is $< 55\%$ for sediment. As the model evaluation time period increases, more stringent acceptability criteria may be warranted. However, the performance metrics and criteria suggested by Moriassi et al. (2007) served as an established point of reference and were used to evaluate the acceptability of model results for this study. It should be noted that *NSE* and *RSR* metrics depend on the absolute values of differences in the timing and magnitudes of measurements and model results and even small differences between measured and simulated peak flows or concentrations will lead to lower skill assessment scores for a model. In contrast, the $|PBIAS|$ metric is less sensitive to differences in timing and magnitude because it depends on the sum of signed differences in measurements and model results.

5. Results and discussion

5.1. Parameter calibration

Hydrological parameters have been measured or calibrated and validated in previous studies (Kinouchi and Musiak, 2008; Wei and Kinouchi, 2014). In this study, data of flow rate was obtained for the period from Jun. 21, 2011 13:00 until Oct. 7, 2013 16:00 at St. M and Dec. 31, 2014 24:00 at St. D. Comparisons between measured and simulated flow rates for these periods are shown in Fig. 3. Table 2 shows the three evaluation criteria for flow rates in 2011–2014. Because $NSE \geq 0.62$, $RSR \leq 0.62$, and $|PBIAS| \leq 18\%$ at St. M and St. D for all four years, the simulated flow rates were acceptable to simulate soil erosion and transport. For soil erosion, the parameters C_f in Eq. (2) and β in Eq. (4) were calibrated based on sensitivity analysis. The flood on Oct. 16, 2013 was firstly used to calibrate the model parameters C_f and β for clay, silt and sand separately, and several candidate combinations

were obtained. The data of total SSCs during the flood on Sep. 22, 2011 (the biggest typhoon event) was used to select the best combination of C_f and β although SSCs for each particle size class was not obtained (Table 1). Instantaneous PSDs were typically measured on an hourly basis at St. D, although data were not obtained during some periods due to equipment problems. SSCs of water grab samples were also used for comparison. Figs. 4(a) and (b) compare simulated and measured SSCs for these calibration periods. Figs. 5(a) and (b) show comparison of simulated and measured SS fluxes for the calibration events.

5.2. Model validation

SSCs of each particle size class measured at St. D for a period in 2013 were used for model validation (Fig. 6). Comparisons of simulated and measured total SS fluxes at St. D for eight individual flood events were also made for validation (Fig. 7). Furthermore, water samples were collected from multiple sites throughout the catchment (Fig. 1) during two flood events in Oct. 2013 for validating the model performance to account for the spatial and temporal variation of SSCs for each particle size class (Fig. 8). Simulated SSCs for the flood event on Oct. 6, 2014 agree well with measurements. SSCs for the flood on Oct. 14, 2014 were overestimated in general, although SSCs were underestimated at St. 3 and St. 5. A possible reason for these differences can be explained by the earlier or delayed time to peak in simulated SSCs at these sites, which results in larger or smaller simulated SSCs, respectively.

A long record of measurements was collected at St. D and St. M. For 2011–2014, the $|PBIAS|$ value for total SS flux at those stations was less

Table 3
Evaluation criteria of simulated total SS flux.

Location	Coefficient	2011	2012	2013	2014
Downstream (St. D)	<i>NSE</i>	0.91	0.22	0.85	0.57
	<i>RSR</i>	0.30	0.89	0.39	0.65
	<i>PBIAS</i>	–4%	–5%	–5%	33%
Middle stream (St. M)	<i>NSE</i>	0.90	–	–	–
	<i>RSR</i>	0.32	–	–	–
	<i>PBIAS</i>	–5%	–	–	–

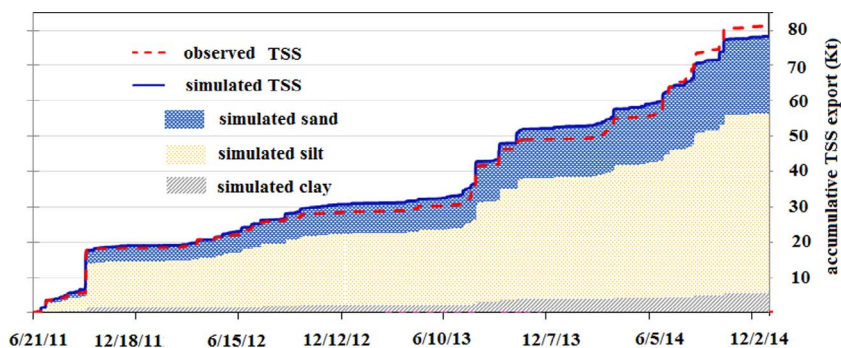


Fig. 9. Comparison between simulated and observed accumulative total SS export from Jun. 21, 2011 to Dec. 31, 2014.

than 33% (Table 3). During 2012, *NSE* and *RSR* acceptability criteria were not satisfied as a consequence of differences in the timing and magnitude of peak sediment concentrations during some events. This was not unexpected because *NSE* and *RSR* metrics depend on the absolute value of differences between measurements and model results. However, the $|PBIAS|$ value for this period was only 5%, indicating that the model is in close agreement with measurements over time. As shown in Fig. 9, simulated total SS transported from the downstream site was 78273 tonnes (t) and is in very close agreement with measured transport (about 81646 t) during the Jun. 21, 2011 to Dec. 31, 2014 monitoring period. From these comparisons of SSCs, fluxes and masses, overall model performance was judged to be acceptable. Our simulation results also show from Mar. 12, 2011, when the accident began, to Dec. 31, 2014, an estimated about 5530 t of clay, 51879 t of silt, 22339 t of sand were eroded from the Kuchibuto River catchment and transport downstream to the Abukuma River (Fig. 9). Overland flows have a smaller transport capacity (C_m) for sand relative to silt. Thus, the mass of sand transported was smaller than silt. Although the transport capacity of clay is larger, the fraction of clay available for transport is small (i.e., supply is limited), so the mass of clay transported was smallest.

5.3. Sediment budget

Soil erosion and transport processes from Jan. 1, 2011 to Dec. 31, 2014 were simulated. Fig. 10 shows the mass balance of SS transport in the catchment for simulation period. Over these four years, the simulated sediment budget indicates that 84632 t of SS was delivered from upland areas to river channels and 80313 t was transported out of the catchment. A relatively small mass of solids was within the channel at the end of the simulations, with 4316 t deposited to the channel bed

and 3 t remaining in suspension. An appreciable amount of sediment deposited onto river bed and was largely comprised of sand, representing roughly 12% of total sand inflow. Because their settling velocity is low, the deposition flux of finer sediments is generally small and relatively little of material eroded from the catchment deposits. In contrast, sands have much higher settling velocities and readily deposit in river channels. Consequently, the “erosion–deposition–resuspension” sequence that occurs for sand transport is different than the “erosion and direct transport” sequence that occurs for clay (Fig. 10). The same phenomenon also occurs in upland areas, where eroded sand mainly deposited on hillsides near the source of erosion. In contrast, clay can be transported for long distances before settling out of suspension such that what clay deposition occurs is largely limited to the floodplain near the river (Fig. 11).

5.4. Critical erosion area identification

The sediment yield was about 155 t/km²/y and is within the range of values estimated in other studies. Based on simulations for 2004 and 2005, Itoshiro et al. (2014) estimated that the annual sediment yield was about 100–200 t/km²/y from tributaries of the Abukuma River watershed. Although weathered granitic material covers most of the Kuchibuto River catchment and other tributary catchments in the western Abukuma River watershed, other factors (e.g., land use) may contribute to soil erosion and transport variations in those catchments. Even within the Kuchibuto River catchment, the sediment yield from different areas varies. According to our simulated results in Table 4, the Middle main stream area supplied more sediment to river channel per unit area (approximately 178 t/km²/y), while the sediment yield (net erosion) or sediment supply ratio (SSR) for the upper main stream area was smaller than the middle portion of the catchment (i.e. the Tributary

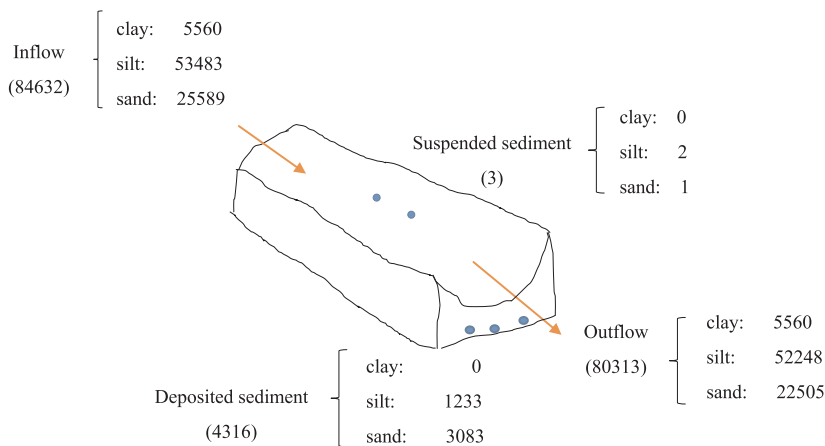


Fig. 10. Mass balance of SS transport in the catchment (unit: t).

* Inflow = Outflow + Suspended sediment + Deposited sediment

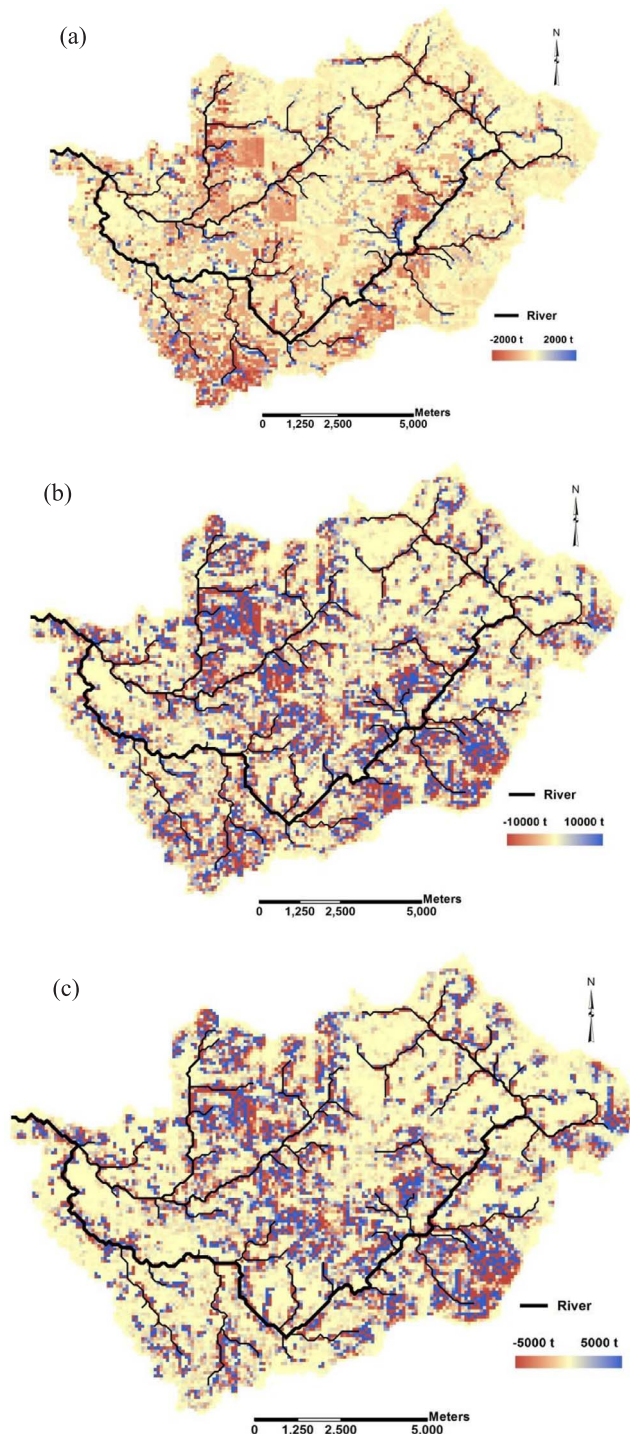


Fig. 11. Simulated net erosion and deposition of (a) clay, (b) silt and (c) sand, from the land surface for the period during Jan. 1, 2011 and Dec. 31, 2014. Negative value means erosion.

and the Middle main stream areas). It indicates the middle portion of the catchment which suffers more serious soil erosion, can be identified as critical erosion areas. The SSR for sub-catchment in the critical erosion areas, such as sub-catchment No. 16, No. 19, No. 17, No. 8, No. 13, No. 20, No. 21, No. 4, No. 5, and No. 11 (Fig. 12), were more than the average sediment yield for the whole catchment (i.e. 155 t/km²/y). Spatial distributions of net erosion and deposition of clay, silt and sand as shown in Fig. 11 also have the same spatial trend.

Multi-site measurements confirm this finding. Based on the

empirical mass budget for measurements in 2011, approximately 56% of sediment and 64% of water generated in the entire catchment passed the St. M and was transported downstream. This indicates that the upper portion of the catchment produced and delivered less sediment than areas further downstream, which generated roughly 44% but only 36% of the flow.

The topographic and land use characteristics are major controlling factors for the sediment yield of most small mountainous rivers (Milliman and Syvitski, 1992; Shi et al., 2014). Our simulation results also suggest that sub-catchments with large agricultural land fraction and steep slopes tend to supply more sediment, while the simulated results include more complicated situations (Table 4). A large SSR was calculated for sub-catchment No. 4, mainly because of steep slope dominating over the sub-catchment although the fraction of agricultural land is small. The fraction of agricultural land of sub-catchment No.20 is slightly higher than that of sub-catchment No.15. However, SSR of No. 20 is more than triple of SSR of No.15. The reason can be partly explained by the volume of surface flow per computational cell in each sub-catchment during the simulation period (Table 4), since more surface flow indicates the larger transport capacity (C_m). There are exceptional cases that are difficult to explain by these factors. For example, the fraction of agricultural land and surface flow volume are smaller in sub-catchment No. 5 than No. 12, but SSR is larger by about 30% than that of No. 12, probably because higher sediment connectivity is achieved in sub-catchment No. 5 due to small catchment size and the direct link of eroding surfaces to streams (De Vente and Poesen, 2005). In Fig. 13 we can see, in the middle portion of the catchment, slopes are very steep. Areas with slopes greater than 15° are rare in upper portions of the catchment but occur much more frequently in the middle part. In our simulations, the SSR in areas with slopes greater than 15° was 412 t/km²/y and 116 t/km²/y in other areas. Slope has a substantial effect on sediment transport capacity, e.g. steeper slopes generally correspond to larger friction slopes (S_f) and consequentially larger transport capacities (C_m). Thus, areas with steep slopes are generally more erosion-prone. Our results show that the SSR in agricultural lands was about 343 t/km²/y, which is much larger than for other land use types (e.g. approximately 64 t/km²/y in forested area). The fraction of vegetation (k_v) in forested lands is usually larger than in agricultural lands. Another factor is flow generation. In forested areas subsurface flow rather than overland flow is expected to be predominant. This combination of factors acts to limit rainfall splash and hydraulic erosion in forested areas, whereas farmland and paddy field land uses supply and deliver more sediment. From upstream to downstream areas, the increasing portion of agricultural land intensifies soil erosion (Fig. 2 and Fig. 11).

5.5. Implication for ¹³⁷Cs migration

Sediment transport processes determine sediment-bound ¹³⁷Cs migration. The ¹³⁷Cs inventory in Fig. 1 shows that the northern part of the Kuchibuto River catchment was more seriously contaminated, especially the upper main river catchment, where decontamination is needed. However, our finding suggests that soil decontamination actions in mid-catchment critical erosion areas are also needed to reduce soil erosion induced ¹³⁷Cs transport downstream to the Abukuma River. Although ¹³⁷Cs is less enriched in coarser particles relative to clays, the greater transport potential of silts and sands in this part of the catchment means that ¹³⁷Cs is more likely to be eroded and eventually transported out of the catchment. The larger deposition areas shown in Fig. 11 represent candidate areas for further field surveys and efforts to control ¹³⁷Cs transport. Kinouchi et al. (2015) reported the ¹³⁷Cs activity of sediments collected using a time-integrated sampler at St. D. Based on the reported ¹³⁷Cs activities, we estimate that the cumulative sediment-bound ¹³⁷Cs transported through the river system (the mass of sediment multiplied by the ¹³⁷Cs activity of sediment) was 346 GBq for the period during Jun.2011–Dec.2012. The distribution of ¹³⁷Cs

Table 4
Sediment erosion in each sub-catchment.

Location	Sub. No.	Area (km ²)	Average slope angle (°)	Fraction of steep slope (> 15°) (%)	Fraction of agricultural land (%)	Volume of surface water flow out of a computational cell (10 ⁴ m ³)	Mass of sediment supply (t)	SSR (t/km ² /y)
Middle mainstream (178 t/km ² /y)	7	2.8	8.30	6	40	3.29	721	64
	16	3.8	<i>10.89</i>	22	48	4.99	5162	337
	19	12.4	<i>10.53</i>	18	25	6.62	10990	222
	17	3.8	<i>13.28</i>	36	25	4.32	3064	203
	8	3.9	9.56	8	34	2.99	2958	188
	13	8.7	<i>10.85</i>	24	24	4.67	6224	179
	20	6.0	5.68	0	51	6.77	4250	178
	21	8.4	8.66	9	37	4.32	5392	160
	18	5.7	5.21	0	61	5.49	3098	136
	14	6.7	7.72	5	40	2.85	3384	127
Upper mainstream (160 t/km ² /y)	15	4.2	6.08	1	48	4.53	846	50
	3	10.9	8.61	7	24	2.79	6190	142
	1	5.5	9.75	12	20	4.00	2719	123
	2	5.3	8.24	4	26	5.92	2006	95
	9	4.7	7.96	4	40	4.88	1757	94
	6	7.8	<i>10.08</i>	16	15	4.32	2595	83
Tributary (112 t/km ² /y)	4	3.1	<i>12.88</i>	34	4	3.52	2592	206
	5	4.1	<i>10.84</i>	20	20	3.55	3025	183
	11	11.7	9.61	17	37	2.83	8488	181
	12	10.5	<i>10.85</i>	21	34	4.18	5997	142
	10	6.8	7.08	3	41	3.57	3174	116
All	–	137	9.21	13	32	4.3	84631	155

The values are italicized if average slope angle ≥ 10°, fraction of steep slope ≥ 16% and fraction of agricultural land ≥ 25%, respectively.

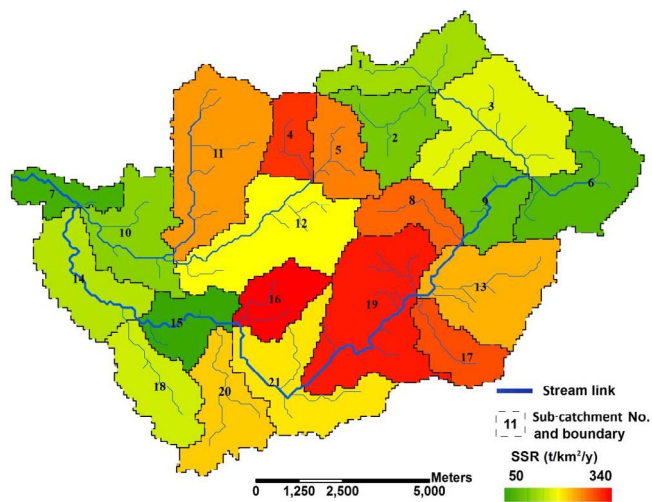


Fig. 12. Sediment supply ratio (SSR) in each sub-catchment.

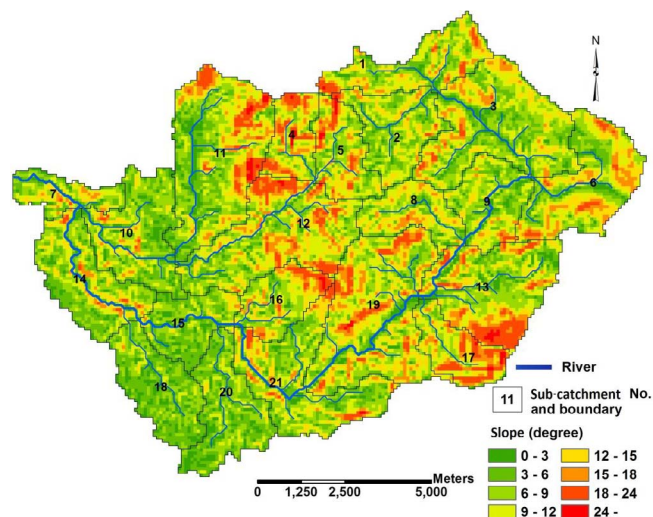


Fig. 13. Slope distribution of the Kuchibuto River catchment.

strongly depends on the initial amount deposited by fallout whereas soil erosion occurs irrespective of the distribution of ¹³⁷Cs. Moreover, the washoff of ¹³⁷Cs from forest canopy plays a significant role in ¹³⁷Cs transport (Kinouchi et al., 2015). Given the prevalence of forested lands in this area, additional research is needed to provide more detailed assessments regarding the transport and fate of ¹³⁷Cs and other radioactive substances in Fukushima region.

6. Summary and conclusions

Soil erosion and transport processes in the Kuchibuto River catchment were simulated for the four-year period Jan. 1, 2011 to Dec. 31, 2014, using the TREX watershed model. Simulated flow rates were found to be acceptable in comparison to measurements for 2011–2014 over the catchment. The correspondence between simulated and measured SS concentrations of water grab samples for multiple sites for flood events and SS concentrations, fluxes and mass at the stations during 2011–2014 demonstrates that model simulations are acceptable. Simulation results also indicate that between Mar. 12, 2011 and Dec.

31, 2014, approximately 5500 t of clay, 52000 t of silt, 22000 t of sand were eroded and transport to the Abukuma River. Model results also indicate that critical erosion areas are located in the middle portion of the catchment, where slopes are steeper and the primary land use is agricultural. Our study suggests that decontamination of soils located in critical erosion areas in the middle portion of the Kuchibuto River catchment would be needed to reduce ¹³⁷Cs transport to the Abukuma River. The results of this study are useful for understanding radiocesium transport at the watershed scale and ultimately for assessing environmental risks.

Acknowledgements

This study was financially supported by Grant-in-Aid for Scientific Research (25110503). The authors also would like to thank Prof. Onda (University of Tsukuba) for supporting on-site monitoring and providing hydrological data.

Reference

- Chino, M., Nakayama, H., Nagai, H., Terada, H., Katata, G., Yamazawa, H., 2011. Preliminary estimation of release amounts of ^{131}I and ^{137}Cs accidentally discharged from the Fukushima Daiichi Nuclear Power Plant into the atmosphere. *J. Nucl. Sci. Technol.* 48, 1129–1134.
- De Vente, J., Poesen, J., 2005. Predicting soil erosion and sediment yield at the basin scale: scale issues and semi-quantitative models. *Earth Sci. Rev.* 71, 95–125.
- Engelund, F., Hansen, E., 1967. A Monograph on Sediment Transport in Alluvial Streams. Teknisk Forlag, Copenhagen, pp. 62.
- Flanagan, D.C., Nearing, M.A., 1995. USDA Water Erosion Prediction Project hillslope and watershed model documentation. NSERL Report No. 10. West Lafayette, Ind.: USDA-ARS National Soil Erosion Research Laboratory.
- Gessler, J., 1965. The beginning of bed load movement of mixtures investigated as natural armoring in Channels. Technical report No. 69, the laboratory of hydraulic research and soil mechanics, Swiss Federal Institute of Technology, Zurich.
- Gessler, J., 1967. The Beginning of Bed Load Movement of Mixtures Investigated as Natural Armoring in Channels. California Institute of Technology, Pasadena, California, pp. 89.
- Gessler, J., 1971. Beginning and ceasing of sediment motion. In: Shen, H.W. (Ed.), *River Mechanics*, Fort Collins, Colorado. pp. 7:1–7:22.
- He, Q., Walling, D.E., 1996. Interpreting particle size effects in the adsorption of ^{137}Cs and unsupported ^{210}Pb by mineral soils and sediments. *J. Environ. Radioact.* 30, 117–137.
- Itoshiro, S., Takemura, K., Kashiwagi, S., Goto, K., Tatsuta, J., Nagasawa, N., Hoshino, T., Mori, Y., Yamanaka, K., 2014. Study on water and substance cycle structure. Report of Japan River Front research Center, No.25.
- Julien, P.Y., Saghafian, B., Ogdien, F.L., 1995. Raster-based hydrologic modeling of spatially-varied surface runoff. *Water Resour. Bull.* 31, 523–536.
- Johnson, B.E., Julien, P.Y., Molnar, D.K., Watson, C.C., 2000. The two-dimensional-upland erosion model CASC2D-SED. *J. Am. Water Resour. Assoc.* 36 (1), 31–42.
- Kinouchi, T., Musiaki, K., 2008. Simulating hydrological impact of environmental change in the Abukuma Watershed, Japan. 4th APHW Conference.
- Kinouchi, T., Yoshimura, K., Omata, T., 2015. Modeling radiocesium transport from a river catchment based on a physically-based distributed hydrological and sediment erosion model. *J. Environ. Radioact.* 139, 407–415.
- Kumar, S., Mishra, A., 2015. Critical erosion area identification based on hydrological response unit level for effective sedimentation control in a river basin. *Water Resour. Manage.* 29, 1749–1765.
- MEXT. 2013. Extension site of distribution map of radiation dose, etc. <http://ramap.jmc.or.jp/map/eng/>.
- Lee, G., Yu, W., Jung, K., APIP, 2013. Catchment-scale soil erosion and sediment yield simulation using a spatially distributed erosion model. *Environ. Earth Sci.* 70, 33–47.
- Morgan, R.P.C., Quinton, J.N., Smith, R.E., Govers, G., Poesen, J.W.A., Auerswald, K., Chisci, G., Torri, D., Styczen, M.E., 1998. The European soil erosion model (EUROSEM): a process-based approach for predicting sediment transport from fields and small catchments. *Earth Surf. Proc. Land.* 23, 527–544.
- Moriassi, D.N., Arnold, J.G., Van Liew, M.W., Bingner, R.L., Harmel, R.D., Veith, T.L., 2007. Model evaluation guidelines for systematic quantification of accuracy in watershed simulations. *Trans. ASABE* 50 (3), 885–900.
- Milliman, J.D., Syvitski, J.P., 1992. Geomorphic/tectonic control of sediment discharge to the ocean: the importance of small mountainous rivers. *J. Geol.* 100, 525–544.
- Sardar, B., Singh, A., Raghuvanshi, N., Chatterjee, C., 2014. Hydrological modeling to identify and manage critical erosion-prone areas for improving reservoir life: case study of Barakar Basin. *J. Hydrol. Eng.* 19 (1), 196–204.
- Shi, Z.H., Huang, X.D., Ai, L., Fang, N.F., Wu, G.L., 2014. Quantitative analysis of factors controlling sediment yield in mountainous watersheds. *Geomorphology* 226, 193–201.
- Srinivasan, R., Arnold, J.G., 1994. Integration of a basin-scale water quality model with GIS. *Water Resour. Bull.* 30 (3), 453–462.
- Tanaka, K., Iwatani, H., Sakaguchi, A., Takahashi, Y., Onda, Y., 2014. Relationship between particle size and radiocesium in river suspended sediment related to the Fukushima Daiichi Nuclear Power Plant accident. *J. Radioanal Nucl. Chem.* 301 (2), 607–613.
- Tanaka, T., Tachikawa, Y., Shiiba, M., Yorozu, K., Kim, S., 2013. Numerical modeling and estimation of radioactive cesium movement at the Kuchibuto river basin, Fukushima. *J. Jpn. Soc. Civil Eng., Ser. B1 (Hydraulic Eng.)* 69 pp. 1_487–1_492.
- Tripathi, M.P., Panda, R.K., Raghuvanshi, N.S., 2003. Identification and prioritization of critical sub-watersheds for soil conservation management using the SWAT model. *Biosyst Eng.* 85, 365–379.
- Velleux, M., England, J., Julien, P.Y., 2008. TRES: spatially distributed model to assess watershed contaminant transport and fate. *Sci. Total Environ.* 404 (1), 113–128.
- Wang, G.Q., Fu, X.D., Shi, H.Y., Li, T.J., 2015. Watershed sediment dynamics and modeling: a watershed modeling system for Yellow River. In: Yang, C.T., Wang, L.K. (Eds.), *Advances in Water Resources Engineering, Handbook of Environmental Engineering*, vol. 14. Springer, Cham Heidelberg New York Dordrecht London, pp. 1–40. http://dx.doi.org/10.1007/978-3-319-11023-3_1. (Chapter 1).
- Wang, G., Wu, B., Li, T., 2007. Digital yellow river model. *J. Hydro-Environ. Res.* 1 (1), 1–11.
- Wei, L., Kinouchi, T., 2014. Improvement of CASC2D model for rainfall-runoff simulation in a forested catchment. *J. Jpn. Soc. Civil Eng., Ser. B1 (Hydraulic Eng.)* 70 (4), 157–162.
- White, M.S., Storm, D.E., Busted, P.R., Stoodley, S.H., Phillips, S.J., 2009. Evaluating nonpoint source critical source area contributions at the watershed scale. *J. Environ. Qual.* 38, 1654–1663.
- Wu, Y., Chen, J., 2012. Modeling of soil erosion and sediment transport in the East River Basin in Southern China. *Sci. Total Environ.* 441, 159–168.
- Wu, Y., Chen, J., 2013. Investigating the effects of point source and nonpoint source pollution on the water quality of the East River (Dongjiang) in South China. *Ecol. Ind.* 32, 294–304.
- Woolhiser, D.A., Smith, R.E., Goodrich, D.C. 1990. KINEROS, A Kinematic Runoff and Erosion Model: Documentation and User Manual. U.S. Department of Agriculture, Agricultural Research Service, ARS-77, 130 p.
- Yamaguchi, M., Maekawa, K., Takeuchi, S., Kitamura, A., Onishi, Y., 2013. Development of a model to predict a radionuclide distribution based on soil migration after Fukushima Dai-ichi Nuclear Power Plant accident. *J. Nucl. Fuel Cycle Environ.* 20, 53–69.
- Yamaguchi, M., Kitamura, A., Oda, Y., Onishi, Y., 2014. Predicting the long-term ^{137}Cs distribution in Fukushima after the Fukushima Dai-ichi nuclear power plant accident: a parameter sensitivity analysis. *J. Environ. Radioact.* 135, 135–146.
- Yamashiki, Y., Onda, Y., Smith, H.G., Blake, W.H., Wakahara, T., Igarashi, Y., Matsuura, Y., Yoshimura, K., 2014. Initial flux of sediment-associated radiocesium to the ocean from the largest river impacted by Fukushima Daiichi Nuclear Power Plant. *Sci. Rep.* 4, 3714. <http://dx.doi.org/10.1038/srep03714>.
- Yoshimura, K., Onda, Y., Sakaguchi, A., Yamamoto, M., Matsuura, Y., 2015. An extensive study of the concentrations of particulate/dissolved radiocesium derived from the Fukushima Dai-ichi Nuclear Power Plant accident in various river systems and their relationship with catchment inventory. *J. Environ. Radioact.* 139, 370–378.